中國機械工程學刊第四十四卷第一期第 99~108 頁(民國一百一十二年)
Journal of the Chinese Society of Mechanical Engineers, Vol.44, No.1, pp 99~108 (2023)

Analytical Approach and Numerical Simulation to Investigate the Stress Field and the Dynamic Stress Intensity Factor of a Cracked-Shaft Under a Periodic Loading

Khemais Hamrouni***, Mohamed Boughazala*, Abdessattar Aloui***
and Mohamed Haddar*

Keywords: Cracked-shaft, periodic loading, dynamic stress intensity factors, stress field.

ABSTRACT

A new analytical formulation was developed to investigate the dynamic behavior of a cracked-shaft subjected to a torsional loading. To validate the effectiveness of the analytical approach a three – dimensional model was designed by the ABAQUS software based on the finite elements method and on the contour integral technique (CIT). A refined mesh was applied in the crack region to better simulate the stress concentration. The variation of the stress intensity factor (SIF) $K_{III,}$ associated with the opening crack mode III, and the stress field in the vicinity of the crack were studied taking into account the effect of both the crack size and the external load. The results show that the values of SIFs KIII become more pronounced when the dimensionless ratio μ exceeds 0.6. The magnitude of SIFs KIII is enhanced from 66.34 MPa.m$^{1/2}$to 110.8 MPa.m$^{1/2}$when the load magnitude is increased from 60N.m to 100N.m. The results of the stress field reveal a good agreement between the analytical results and the FEM findings with an acceptable error that does not exceed 5%.

INTRODUCTION

Shafts are among the most important mechanical components and are widely used in the rotating machines such as turbines, rotors, and compressors. They often work in severe conditions and are therefore subjected to progressive deterioration such as crack, wear, etc. These defects limit the safety of shafts and produce economic problems since they affect the reliability of the mechanical system. Furthermore, the presence of the crack might have destructive effects on the rotor system if it is not detected in time. Thus, a timely detection of a shaft crack would potentially avoid severe damages and expensive repairs as well as assuring the safety of the staff. Consequently, the study of the dynamic behavior of a rotating shaft containing a transverse crack has been the subject of large investigations, in the last four decades, owing to its significant role in fault detection analysis. Dimarogonas (1983, 1996) investigated the effect of the crack on the dynamic response of a cracked rotating shaft taken into consideration the local flexibility of the cracked section. Papadopoulos and Dimarogonas (1987, 1992) have extensively reported the issue of vibrations due to crack. They proposed the presence of either of longitudinal, bending or torsional vibrations in the cracked shaft. Moreover, important efforts have been made to produce relevant numerical, analytical and experimental results. Rubio et al. (2015) developed a numerical model using the finite element method (FEM) to calculate the stress intensity factors (SIF_s) along the crack front of a rotating cracked shaft. A new analytical model is developed in another work of Rubio et al. (2019) to obtain the stress intensity factors at any position of the front of a crack contained in a rotating shaft as a function of the position on the front, the rotation angle and the crack geometric parameters (shape and depth). Two nodded Timoshenko beam elements with four degrees of freedom (DOFs) per node are used by Gayen et al. (2017) to model a functionally graded (FG) shaft having multiple cracks. The translational and rotary inertia, transverse shear deformations and gyroscopic moments are considered in finite elements (FE) formulation to study the effects of location, orientation and size of cracks on the dynamic response of such shafts. Li et al. (1989) presented a new concept results from an analytic-

Paper Received February, 2022. Revised May, 2022, Accepted August, 2022, Author for Correspondence: Mohamed Boughazala.

* *Professor, Mechanics, Modelling and Manufacturing Laboratory (LA2MP), Mechanical Engineering Department, National Engineers School of Sfax, B.P. W3038, Sfax, Tunisia.*
** *Associate Professor, Higher Institute of Applied Sciences and Technology, University of Gabes, Tunisia.*

experimental approach to evaluate the local stiffness reduction of the cracked shaft. A finite elements analysis is carried out by Sekhar and Prabhu (1994) in order to investigate the vibration characteristics of a simply supported shaft with a transverse crack and to study the bending stress fluctuations. In the same context Chatterton et al. (2019) considered an appropriate tridimensional FE model to estimate the stresses distribution in the cracked section of a shaft of a real steam turbine. Bachschmid et al. (2008) created a simplified model in order to simulate the dynamic behavior of a rotating cracked shaft. This approximated model has been used to calculate the stiffness variations of the cracked shaft as well as the additional vibrations due to the crack. Based on an energy analysis, Gómez et al. (2016) presented an analytical model to detect the crack in a rotating shaft. Thereafter, experimental measurements were performed for a rig comprising a cracked shaft under a range of fault conditions and at different rotational speeds. Kumar et al. (2015) considered a steel shaft supported on two bearings at both ends in order to experimentally examine the vibration characteristics of a cracked shaft. Furthermore, a simplified model was designed using ANSYS software and the harmonic analysis was performed for various combinations of crack depths and crack locations. An analytical solution based on the variational formulation and a numerical finite elements model were reported by Chondros and Labeas (2007) to analyze the torsional vibration and crack identification for a cracked cylindrical shaft. Recently, in a new study, El Arem (2021) explored the vibrational behavior of rotating shaft containing a cracked transverse section at mid − span by considering a three dimensional structure under applied forces. Hosseini et al. (2005) presented a numerical technique for the calculation of stress intensity factors as a function of time for coupled thermo-elastic problem. Theocaris et al. (1980) used path-independent integrals around crack tips to estimate stress intensity factors at crack tips in plane elasticity static problems. Miyazaki (1991) proposed a method based on a line-spring model to calculate the dynamic stress intensity factor of a pre-cracked three-point bending specimen and a pre-cracked four-point bending specimen. Chen (1975) used the time-dependent Lagrangian finite-difference code (HEMP) to compute the stress intensity factor for a centrally cracked rectangular bar. In light of the review above, the dynamic SIF and the stress field in the vicinity of the crack were not extensively studied when a shaft crack appeared and the stress concentration was observed. This needs to be deeply studied. To this end, the main objective of this paper was to investigate the effects of the external load and the crack depth on the variation of the SIFs K_{III} associated with the mode III and on the stress field around the crack. Accordingly, an analytical formulation solved by the Newmark iterative schema and a numerical simulation based in the ABAQUS software were used and some conclusions were drawn in the conclusive section.

ANALYTICAL APPROACH

Cracked -Shaft Modeling

A steel elastic shaft of length (L) and radius (R) was modeled by a variable section $S(x)$. The shaft containing a transverse crack of depth (a). The crack is located at a distance (x_c) from the left end and is lying on a plane normal to the shaft axis and having a straight front. The cracked shaft is subjected to a dynamic torsional moment $M_0(t) = m\,sin\,\omega\,t$applied in the right end. A schematic representation, showed the boundary conditions and the periodic moment acting on the cracked shaft, is presented in Figure 1.

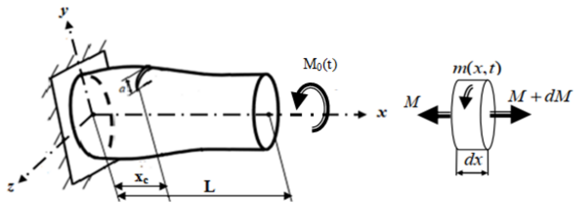

(b) **(a)**

Fig. 1. (a). Cracked- shaft with the boundary conditions; (**b**).Elemental disc of the shaft.

Consider an elemental disc of the shaft with length (dx) (Fig. 1.b) subjected to an external moment per unit length$m(x,t)$. M and $M+dM$ are respectively the torsional moments at the left and right section of the element.

The dynamic equilibrium of this element gives:

$$dM + m(x,t)dx = \theta(x)dx\frac{\partial^2\varphi(x,t)}{\partial t^2}, \qquad (1)$$

Where $\theta(x)$ is the moment of inertia per unit length of the shaft and $\varphi(x,t)$is the torsional angle according to the abscise x and time t. The relationship between torsional angle, the torsional moment and the material properties is,

$$\frac{\partial\varphi(x,t)}{\partial x} = \frac{M}{GI_P(x)} \qquad (2)$$

G is the shear modulus, $I_p(x)$ is the quadratic polar moment; we can write:

$$\frac{\partial M}{\partial x} = G\frac{\partial}{\partial x}\left(I_p(x)\frac{\partial\varphi(x,t)}{\partial x}\right) \qquad (3)$$

The dynamic motion equation of the uncracked shaft can be written as,

$$G\frac{\partial}{\partial x}\left[(I_P(x)\frac{\partial\varphi(x,t)}{\partial x}\right] + m(x,t) = \theta(x)\frac{\partial^2\varphi(x,t)}{\partial t^2} \qquad (4)$$

The quadratic polar moment, for the cracked-shaft, will be reduced by ΔI_Pusing these functions:

$$\delta(x - x_c) = \begin{cases} 1 x = x_c \\ 0 x \neq x_c \end{cases}$$

$$\delta(x-x_m)=\begin{cases}1 x = x_m\\ 0 x \neq x_m\end{cases} \quad (5)$$

The dynamic equation of the cracked shaft is:

$$\frac{\partial}{\partial x}\left[G(I_P(x)-\Delta I_P\delta(x-x_c))\frac{\partial\varphi(x,t)}{\partial x}\right]+m(x,t)\delta(x-x_m)=\theta(x)\frac{\partial^2\varphi(x,t)}{\partial t^2} \quad (6)$$

The kinetic energy *T* and potential strain energy *U* can be written respectively as,

$$T=\frac{1}{2}\int_0^l\theta(x)\left[\frac{\partial\varphi(x,t)}{\partial t}\right]^2dx \quad (7)$$

$$U=\frac{1}{2}\int_0^l G\left(I_P(x)-\Delta I_P\delta(x-x_c)\right)\left[\frac{\partial\varphi(x,t)}{\partial x}\right]^2dx \quad (8)$$

The work achieved by the moment *M(t)* is:

$$W=\int_0^l m(x,t)\delta(x-x_m)\,\varphi(x,t)dx$$

$$=M_0(t)\varphi(x_m,t) \quad (9)$$

The solution of the dynamic equation (6) can be expressed in the following form:

$$\varphi(x,t)=\sum_{i=1}^{\infty}\phi_i(x)q_i(t)) \quad (10)$$

where, $\phi_i(x)=sin\frac{i\pi x}{2l}$ is a function which satisfy the boundary conditions of the beam such as:

$$\varphi(0,t)=0 \quad (11)$$

Then, we get:

$$T=\frac{1}{2}\int_0^l\theta(x)\left[\sum_{i=1}^{\infty}\phi_i(x)\dot{q}_i(t)\sum_{j=1}^{\infty}\phi_j(x)\dot{q}_j(t)\right]dx$$

$$=\frac{1}{2}\sum_{i=1}^{\infty}\sum_{j=1}^{\infty}\dot{q}_i(t)m_{ij}\dot{q}_j(t) \quad (12)$$

$$U=\frac{1}{2}\int_0^l G\left(I_p(x)-\Delta I_p\delta(x-x_c)\right)\left(\sum_{i=1}^{\infty}\frac{\partial\phi_i(x)}{\partial x}q_i(t)\sum_{j=1}^{\infty}\frac{\partial\phi_j(x)}{\partial x}q_j(t)\right)dx=\frac{1}{2}\sum_{i=1}^{\infty}\sum_{j=1}^{\infty}q_i(t)\,k_{ij}q_j(t)-\frac{1}{2}\sum_{i=1}^{\infty}\sum_{j=1}^{\infty}q_i(t)\,k^*{}_{ij}q_j(t) \quad (13)$$

$$W=\sum_{i=1}^{\infty}M_0(t)\phi_i(x_m)\,q_i(t)$$

$$=\sum_{i=1}^{\infty}f_i(t)\,q_i(t) \quad (14)$$

with,

$$m_{ij}=\int_0^l\theta(x)\phi_i(x)\phi_j(x)dx \quad (15)$$

$$k_{ij}=\int_0^l GI_p(x)\frac{\partial\phi_i(x)}{\partial x}\frac{\partial\phi_j(x)}{\partial x}dx \quad (16)$$

$$k^*{}_{ij}=\int_0^l G\Delta I_p\delta(x-x_c)\frac{\partial\phi_i(x)}{\partial x}\frac{\partial\phi_j(x)}{\partial x}dx$$

$$=G\Delta I_p\frac{\partial\phi_i(x)}{\partial x}\frac{\partial\phi_j(x)}{\partial x}\bigg|_{x=x_c} \quad (17)$$

$$f_i(t)=M_0(t)\phi_i(x_m) \quad (18)$$

Using Lagrange's equation:

$$\frac{d}{dt}\left(\frac{\partial T}{\partial\dot{q}_i}\right)-\frac{\partial T}{\partial q_i}+\frac{\partial U}{\partial q_i}=\frac{\partial W}{\partial q_i} \quad (19)$$

We obtain the following system of equations:

$$\sum_{j=1}^{\infty}m_{ij}\,\ddot{q}_j(t)+\sum_{j=1}^{\infty}\left(k_{ij}-k^*\right)q_j(t)=f_i(t) \quad (20)$$

What we can write in matrix form:

$$[M]\underline{\ddot{q}}(t)+([K]-[K^*])\underline{q}(t)=\underline{f}(t) \quad (21)$$

for $i=1,\ldots,n$ and $j=1,\ldots,n$, we get:

$$[M]=[m_{ij}],[K]=[k_{ij}],[K^*]=[k^*{}_{ij}] \quad (22)$$

$$\underline{q}(t)=\{q_1(t),\ldots,q_n(t)\}^t,(t)=\{f_1(t),\ldots,f_n(t)\}^t \quad (23)$$

Using Newmark's Method of Direct Integration and we adopt the notation: $\underline{q}(t)=\underline{q}_t$, we get:

$$\begin{cases}\underline{q}_t=\underline{q}_{t-\Delta t}+\Delta t\underline{\dot{q}}_{t-\Delta t}+\frac{\Delta t^2}{2}\underline{\ddot{q}}_{t-\Delta t}+\beta\Delta t^3\,\underline{\dddot{q}}_{t-\Delta t}\\ \underline{\dot{q}}_t=\underline{\dot{q}}_{t-\Delta t}+\Delta t\underline{\ddot{q}}_{t-\Delta t}+\gamma\Delta t^2\,\underline{\dddot{q}}_{t-\Delta t}\end{cases} \quad (24)$$

The implicit method, for $\beta=\frac{1}{4}$ and $\gamma=\frac{1}{2}$, is unconditionally stable and has proved to be one of the most popular methods in structural dynamics.

Using the approximation $\underline{\dddot{q}}_{t-\Delta t}=\frac{\ddot{q}_t-\ddot{q}_{t-\Delta t}}{\Delta t}$ we can write:

$$\begin{cases}\underline{q}_t=\underline{q}_{t-\Delta t}+\Delta t\underline{\dot{q}}_{t-\Delta t}+(\frac{1}{2}-\beta)\Delta t^2\underline{\ddot{q}}_{t-\Delta t}+\beta\Delta t^2\underline{\ddot{q}}_t\\ \underline{\dot{q}}_t=\underline{\dot{q}}_{t-\Delta t}+(1-\gamma)\Delta t\underline{\ddot{q}}_{t-\Delta t}+\gamma\Delta t\underline{\ddot{q}}_t\end{cases} \quad (25)$$

or as the following form:

$$\begin{cases}\underline{\ddot{q}}_t=b_1(\underline{q}_t-\underline{q}_{t-\Delta t})+b_2\underline{\dot{q}}_{t-\Delta t}+b_3\underline{\ddot{q}}_{t-\Delta t}\\ \underline{\dot{q}}_t=b_4(\underline{q}_t-\underline{q}_{t-\Delta t})+b_5\underline{\dot{q}}_{t-\Delta t}+b_6\underline{\ddot{q}}_{t-\Delta t}\end{cases} \quad (26)$$

$b_1=\frac{1}{\beta\Delta t^2}$, $b_2=\frac{-1}{\beta\Delta t}$, $b_3=1-\frac{1}{2\beta}$, $b_4=\frac{\gamma}{\beta\Delta t}$, $b_5=1-\frac{\gamma}{\beta}$, $b_6=(1-\frac{\gamma}{2\beta})\Delta t$

The differential equation (21) becomes:

$$[b_1M+(K-K^*)]\,\underline{q}_t=\underline{f}(t)+[M]\left(b_1\underline{q}_{t-\Delta t}-b_2\underline{\dot{q}}_{t-\Delta t}-b_3\underline{\ddot{q}}_{t-\Delta t}\right) \quad (27)$$

It is an equation which its form can be written as:

$$[\bar{K}]\underline{q}_t=\bar{F}_t \quad (28)$$

Where $[\bar{K}]=[b_1M+(K-K^*)]$,is the fictive matrix of rigidity

and

$\bar{F}_t = \underline{f}(t) + [M]\left(b_1\underline{q}_{t-\Delta t} - b_2\underline{\dot{q}}_{t-\Delta t} - b_3\underline{\ddot{q}}_{t-\Delta t}\right)$, is a fictive force.

The initial conditions are:

$$\underline{q}_0 = \vec{0}, \underline{\dot{q}}_0 = \vec{0}, \underline{\ddot{q}}_0 = \vec{0} \quad (29)$$

We use the Newmark's iterative schema with increments of time $(t = \Delta t, 2\Delta t, 3\Delta t, \ldots N\Delta t)$ to determine the vector $\underline{q}_t = (q_1(t), \ldots, q_i(t), \ldots, q_n(t))$, then we determine the function $\varphi(x,t)$ using equation (10).

Stress Field and Dynamic Stress Intensity Factor

$$\sigma_{ij}(r,\psi,t) = \frac{1}{\sqrt{2\pi r}}\begin{bmatrix} K_I(t)f_{ij}(\psi) + K_{II}(t)g_{ij}(\psi) + \\ K_{III}(t)h_{ij}(\psi) \end{bmatrix} \quad (30)$$

$K_I(t)$, $K_{II}(t)$ and $K_{III}(t)$ are the stress intensity factors associated respectively with the cracking modes I, II, and III.
The stress intensity factor defines the magnitude of the local stresses around the crack tip. It depends on loading, crack size, crack shape, and boundary conditions of the structures. The dynamic stress intensity factor for an isotropic material can be derived by calculating the stress field according to the polar coordinates (r,ψ) at the crack tip (Figure 2), (Sladek et al., 1997; Sony et al., 2006).

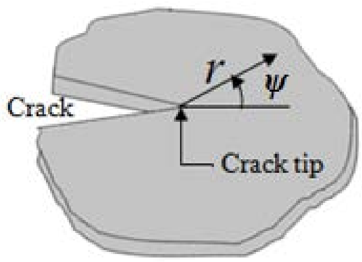

Fig. 2. Polar coordinates at a crack tip.

In our case we have the mode III crack opening; it will be described with the dynamic stress intensity factor $K_{III}(t)$, we get (Hahn, 1976):

$$\tau(r,\psi,t) = \frac{K_{III}(t)}{\sqrt{2\pi r}} \cos\frac{\psi}{2} \quad (31)$$

$K_{III}(t)$ can be expressed by the following relation,

$$K_{III}(t) = \tau(x_c,t)\sqrt{\pi a}\,Y \quad (32)$$

Y=f(a) is a correction factor, which depends of the crack depth and $\tau(x_c,t)$ is the nominal shear stress calculated from the following equation:

$$\tau(x,t) = G\frac{\partial\varphi(x,t)}{\partial x}R_c|x = x_c \quad (33)$$

For $\psi = 0$ and $r = r_0$, the nearest point of the crack tip, we can calculate the approximate value of the correction factor by using equations (31) and (33) as follow:

$$Y = \frac{\tau(r_0,t)}{\tau(x_c,t)}\sqrt{\frac{2r_0}{a}} \quad (34)$$

THE FINITE ELEMENTS SIMULATION

In order to analyze numerically the dynamic behavior of a cracked shaft, a 3D model was built and simulated. The transverse crack is assumed to be located at the middle of the shaft and it extends along the cross section with a uniform depth distribution. The boundary conditions of the cracked- shaft can be set so that the left end is fixed and the right end is free (Figure 3).

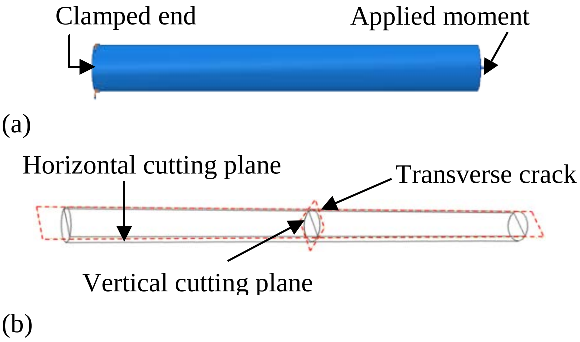

Fig.3. 3D model of the shaft, **(a).** The boundary condition; **(b).** Position of imaginary cutting planes respect to crack.

The model, which mechanical and geometrical parameters are illustrated in Table 1, is selected to check the effectiveness and the validity of the analytical results. This model can be modified accordingly in order to study different crack depths and varying loading values.

Table 1. Cracked shaft parameters.

Parameter	Notation	Value
Young modulus (GPa)	*E*	210
Shear modulus (GPa)	*G*	80
Density (kg/m3)	ρ	7800
Poisson's ratio	ν	0.3
Length of the shaft (mm)	l	254
Diameter of the shaft (mm)	d	18.5

The FE model includes 768784 nodes and 737108 linear hexahedral elements of type C3D8R (8 nodes linear brick elements). To better produce the stress singularity and obtain more accurate results in this article, the mesh of this model was refined in the area near to the cracked section and the rest was designed so as not to be too dense and the elements would not be too distorted as shown in Figure 4.

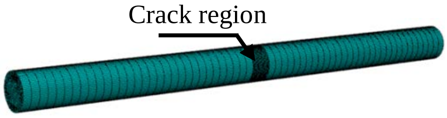

Fig. 4.a. Finite elements model of the cracked shaft.

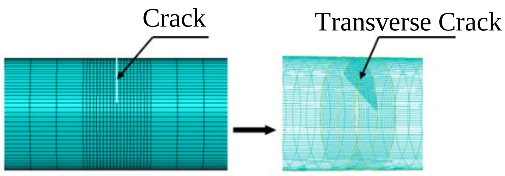

Fig. 4.b. Enlarged view of the refined mesh.

RESULTS AND DISCUSSION

Stress Concentration

To extract the dynamic stress intensity factor and the stress field, dynamic simulation was used based in The Contour Integral Method. Likewise this method was applied in order to clearly show the concentration of the stress in the vicinity of the crack as shown in Figure 5.

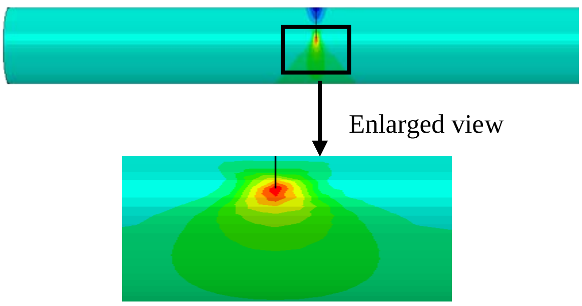

Fig.5. Stress concentration.

Considered $\mu = \frac{a}{R}$ is the dimensionless parameter of crack depth, where a defines the crack depth and R is the shaft radius. Figure 6 represents the cross section of the cracked shaft at the position (X_c = 127mm), in the cases where (μ= 0.2, 0.4, 0.6, 0.8) and the moment (mt= 80N.m). These figures clearly show the stress concentration near the crack tip at the two ends of the crack front.

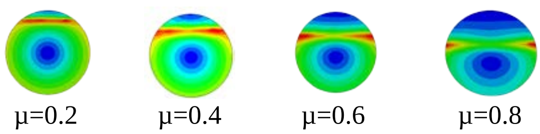

Fig.6. Cross section of the cracked shaft in different crack depths.

Figure 7 clearly shows that the stress concentration in the vicinity of the crack increases with the enlargement of the crack size. Thus, in the case of the largest crack depth (μ=1), a very significant stress concentration was observed at the crack tip.

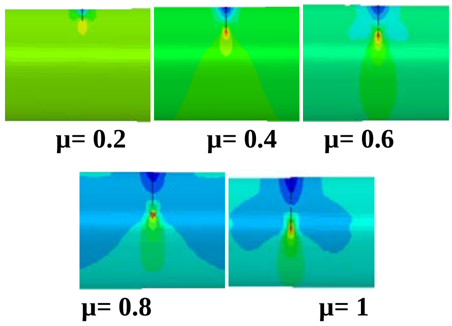

Fig.7. Effect of crack size on the stress concentration.

Twist Angle

Based in the Newmark method, the twist angle of the shaft is computed using MATLAB software. Figures 8 and 9 illustrate, respectively, the evolution of the twist angle for various time and position.

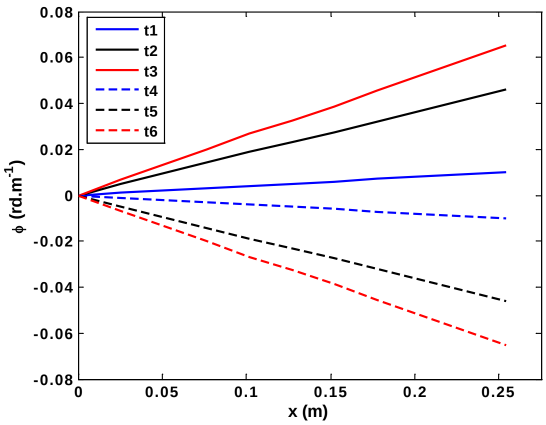

Fig.8. Variation of the twist angle in different values of time (t1= 0.025s, t2= 0.125s,t3= 0.25s, t4= 0.525s, t5= 0.625s, t6= 0.75s).

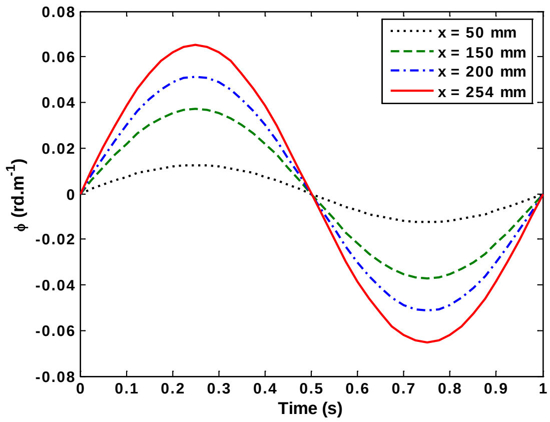

Fig.9. Variation of the twist angle with time.

Stress Intensity Factor

The SIF is a failure criterion that depends on the geometry of the shaft, the crack depth as well as the applied loading (Boughazala et al., 2019). The dynamic SIF for mode III was investigated relating to changes in crack size and applied loading.

As shown in Figure 10, different mesh sizes have been used in order to prove the convergence of the results.

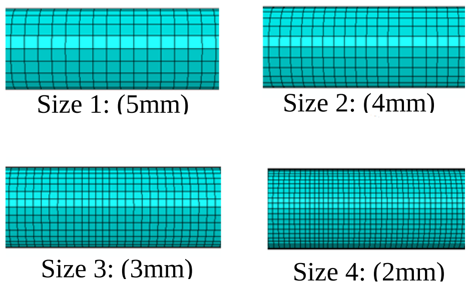

Fig. 10. Different sizes of a mesh element.

Table 2 illustrated the influence of the mesh size on the values of KIII. It can be observed, through this table that almost the same results were found for the different meshes with a maximum error which does not exceed 1. 5%.

Table 2. Effect of the mesh on the KIII (μ=0.6).

	Size 1 (5mm)	**Size 2 (4mm)**	**Size 3 (3mm)**	**Size 4 (2mm)**	**Max. error**
mt= 60N.m	67.348	66.781	66.348	66.291	1.5%
mt= 70N.m	78.412	77.830	77.406	77.286	1.45%
mt= 80N.m	89.544	88.903	88.464	88.311	1.39%

In Figure 11, different crack sizes are selected to study the effect of crack depth on the SIF K_{III} for a constant load (mt= 80N.m) with respect to the crack position. The Stress intensity factor has been calculated around the vicinity of the crack tip (r = 0.25 mm).As well shown in this figure the SIF's values were influenced by the growth of crack's size. It also showed that this effect becomes more pronounced when the dimensionless crack depth μ exceeds 0.6.

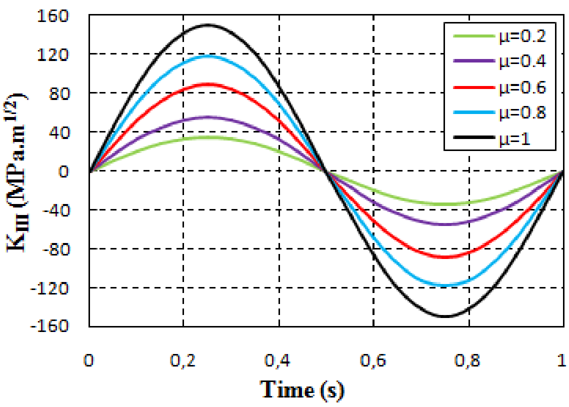

Fig. 11. Evolution of K_{III} according to the crack depth.

Assuming that the dimensionless parameter μ=0.6, the other parameters are fixed and only the load magnitude is varied from 60N.m to 100N.m with the interval of 10N.m.The SIFs variation depending on different periodic moment values are illustrated in Figure 12.

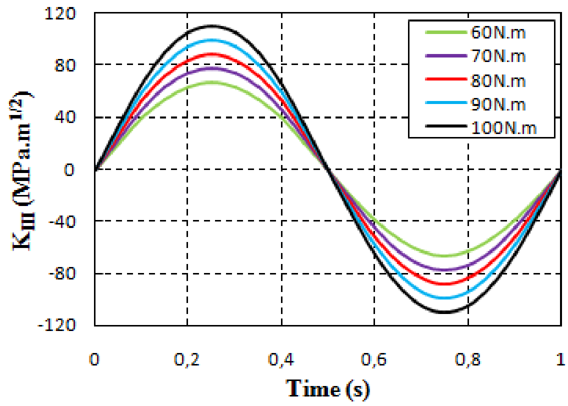

Fig. 12. Evolution of K_{III} according to the load.

It can be observed from Figs.11 and 12 that when a crack appears, the magnitude of SIFs KIII is enhanced with the increasing of the crack depth and the applied load. This is because the cracked-shaft loses much rigidity and becomes more and more flexible with the load and crack depth load increase.

Stress Field

Figure 13presents, through five cases, the effect of crack depth on the stress field in the vicinity of crack by analytical and numerical methods. From this figure we can observe that the trends of the stress are parabolic; this explains that the stress values will decrease obviously when we are far from the crack. Furthermore, it can be seen that the longer the crack is, the more severe the stress concentration becomes. Also, it is clear that in case which represents a deep crack depth ratio (μ=1), the levels of the stress increase significantly compared to that of case which is a smaller crack depth ratio (μ=0.2).

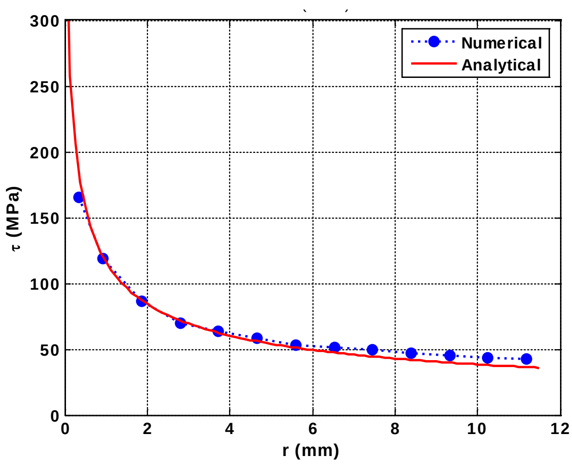

Case 1: μ= 0.2

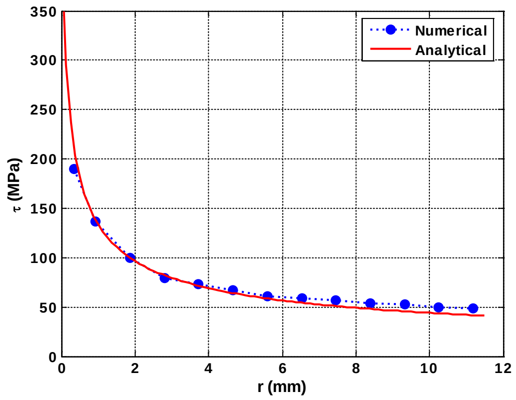

Case 2: μ=0.4

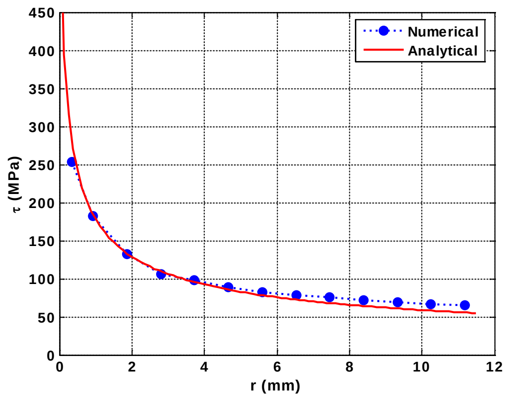

Case 3: μ= 0.6

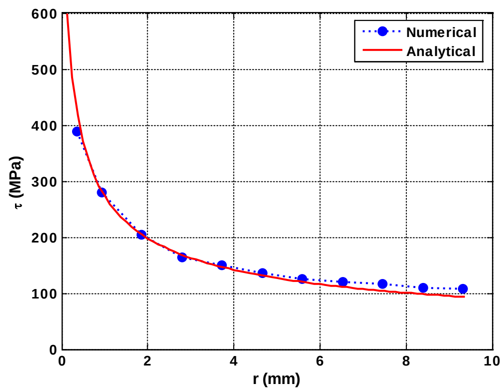

Case 4: μ=0.8

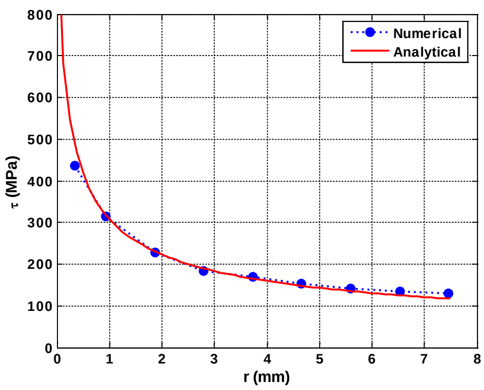

Case 5: μ=1

Fig. 13. Stress variation with the crack depth.

As shown in Figure 14, the effect of applied moment on the cracked shaft is investigated by two methods. Thus, five cases were considered. Each of these cases is related to a different value of dynamic moment for a constant crack depth ratio (μ=0.8).

It can be determined, through Figs. 13 and 14 that the magnitudes of the stress rise with both the applied load and the crack depth increase. Moreover, the crack depth plays a more important role than the applied load in the growth of the stress concentration in the crack region. This clearly proves that the stress changes according to the crack depth rather than to the load. Results of the stress field presented in Figs. 13 and 14 have shown a good agreement between the analytical formulations and the numerical findings. These results prove that the analytical approach developed in this paper will be a major step to analyze the dynamic behavior for realistic industrial systems.

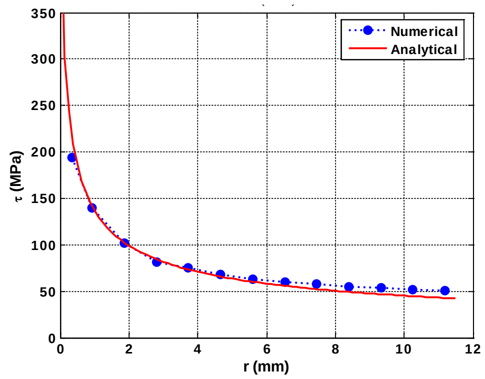

Case 1: mt= 60 N.m

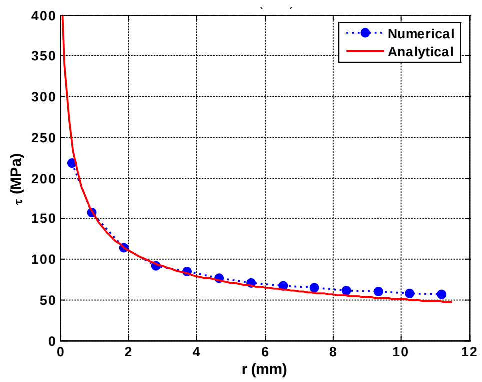

Case 2: mt=70N.m

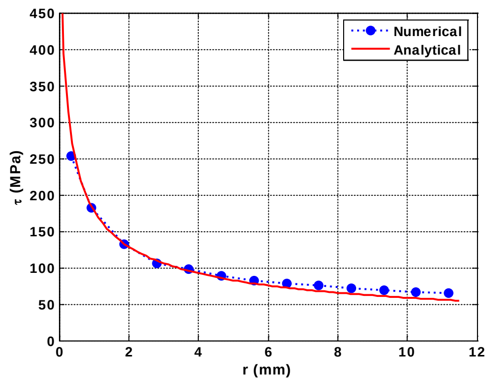

Case 3: mt= 80 N.m

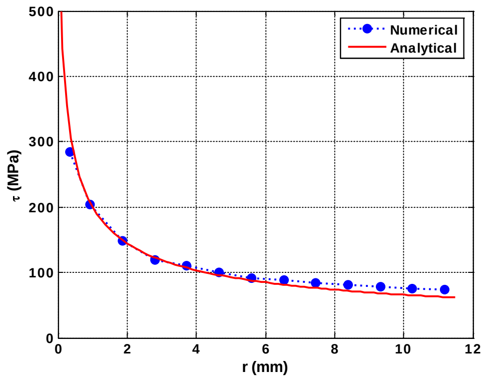

Case 4: mt=90N.m

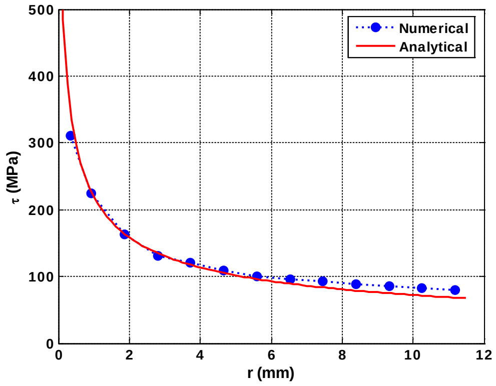

Case 5: mt=100N.m

Fig. 14. Stress variation with load.

Relative Discrepancy Between Analytical and Numerical Results

Table 3 illustrates the relative discrepancies between the values of the stresses' field under the loads (mt=60Nm and 70Nm) obtained with the analytical formulation and the numerical simulation (case1 and case 2 in Fig.14). It can be noted that almost the same results of stresses field were found for both analytical and numerical methods with a tolerable error that varies between 0. 29% and 4.48% (for mt=60 Nm) and between 0. 2% and 4.68% (for mt=70 Nm).

Figure 15 displays the evolution of the discrepancy between analytical and numerical results over a distance of 6.5 mm from the crack tip for two cases (mt=60Nm and mt=70Nm). According to this curve, it can be observed that the discrepancy does not exceed 5% in both cases and the average discrepancy between the two methods is 2.14% for mt=60Nm and 2.08% for mt=70Nm. This accordance demonstrates clearly the reliability of the analytical approach.

Table 3. Discrepancy between analytical and numerical results.

r	**0.250**	**0.933**	**1.866**	**2.798**	**3.730**	**4.662**	**5.594**	**6.525**
Stress Anal60	204.60	145.45	102.36	80.41	75.69	67.89	60.69	57.56
Stress Num60	196.41	144.11	100.24	81.32	75.91	68.92	62.83	60.14
Stress Anal70	230.16	162.62	156.60	111.15	91.44	83.42	73.83	65.63
Stress Num70	221.42	161.11	153.81	112.44	91.62	84.85	76.11	68.70
ε_{60}(%)	**4.17**	**0.93**	**1.10**	**1.13**	**0.29**	**1.52**	**3.53**	**4.48**
ε_{70} (%)	**3.95**	**0.75**	**1.16**	**1.16**	**0.20**	**1.71**	**3.09**	**4.68**

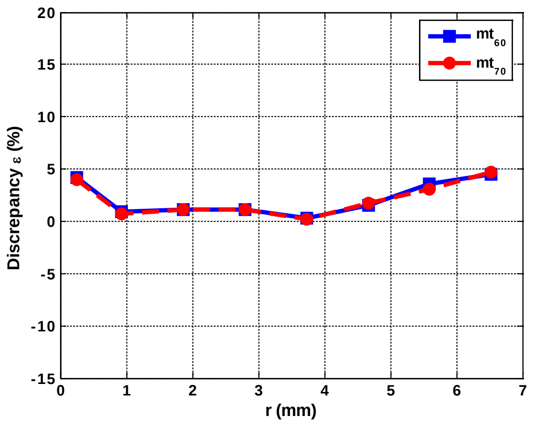

Fig. 15. Discrepancy evolution.

CONCLUSION

Analytical approach and finite elements method were used in this study in order to determine the dynamic stress intensity factor for mode III as well as the stress field at the crack tip, taking into account the influence of the applied load and the variation of the crack depth. The obtained results from the two methods have shown a good accordance and the following conclusions can be forwarded:

- The stress intensity factor K_{III} increases with the increase of both the crack depth and the applied load.
- The effect of the crack depth on K_{III} appeared to be greater than that of the applied load.
- The finite elements analysis, using ABAQUS software is considered as a reliable and efficient tool to validate the analytical results and to solve the dynamic problems. Interestingly, this analytical

approach plays an important role in connecting the fundamental research and the practical usage, and it can be extended in future studies in order to describe 3D dynamic problems arising in other types of defects.

ACKNOWLEDGEMENT

This work has been supported by the Mechanics, Modeling and Production Laboratory of the National Engineering School of Sfax (Tunisia).

REFERENCES

Bachschmid, N., Tanzi, E. and Audebert, S., “The effect of helicoidal cracks on the behaviour of rotating shafts,”*Eng. Frac. Mech.s*.,Vol. 75, pp. 475–488 (2008).

Boughazala, M., Hamrouni, k. et al.,“Analytical approach and numerical simulation to investigate the stress field and the dynamic stress intensity factors of a cracked tooth subjected to a periodic loading,”*Mechanics & Industry*.,Vol. 20, 629, (2019).

Chatterton, S., Pennacchi, P. et al.,“Analysis of the periodic breathing of a transverse annular crack propagated in a real rotating machine,” *Eng. Fail. Anal*.,Vol. 99, pp. 126-140 (2019).

Chen, Y.,“Numerical computation of dynamic stress intensity factors by a lagrangian finite-difference method,” *Engineering fracture mechanics*.,Vol. 7, pp. 653-660 (1975).

Chondros, T. and Labeas, G.,“Torsional vibration of a cracked rod by variational formulation and numerical analysis,” *Journal of Sound and Vibration*.,Vol. 301, pp. 994–1006 (2007).

Dimarogonas, A.., and Papadopoulos, C.,“Vibration of cracked shafts in bending,”*J. of Sou.and Vib.*.,Vol. 91, No. 4, pp. 583–593 (1983).

Dimarogonas, A.D.,“Vibration of cracked structures: a state of the art review,”*Eng. Fract.Mech*.,Vol. 55, pp. 831–57 (1996).

Gayen, D., Chakraborty, D.et al., “Finite element analysis for a functionally graded rotating shaft with multiple breathing cracks,” *Int. J.Mech*.,Vol. 134, pp.411–23 (2017).

Gómez, M., Castejón, C. et al.,“Crack detection in rotating shafts based on 3× energy: Analytical and experimental analyses,” *Mechanism and Machine Theory*.,Vol. 96, pp. 94–106 (2016).

Hahn, H.G., Bruchmechaik. Einfuehrung in die theoretischen grundlagen; Stuttgart (1976).

Hosseini, P.et al.,“Boundary element analysis of stress intensity factor in some two-dimensional dynamic thermo-elastic problems,” *Engineering Analysis with Boundary Elements*.,Vol. 29, pp. 232-240 (2005).

Kumar, S., Harikrishna, Ch. et al.,“Dynamic analysis of a cracked rotor- an experimental and finite element investigation,” *Materials Today: Proceedings*.,Vol. 2, pp. 2131–2136 (2015).

Li, C., Bernasconi, O. and Xenophontidis, N.,“A generalized approach to the dynamics of cracked shafts,”*Journal of Vibration, Acoustics, Stress, and Reliability in Design*.,Vol. 111, pp. 257-263 (1989).

Miyazaki, N.,“Application of line-spring model to dynamic stress intensity factor analysis of pre-cracked bending specimen,” *Eng. Frac. Mech.*., Vol. 38, pp. 321-326 (1991).

Papadopoulos, C. and Dimarogonas, A., “Coupling of bending and torsional vibration of a cracked Timoshenko shaft,” *Ingenieur-Archiv*.,Vol. 57, pp. 257–266 (1987).

Papadopoulos, C. and Dimarogonas, A.,“Coupled vibration of cracked shafts,” *J. of Vib. and Acou.*.,Vol. 114, pp. 461–467 (1992).

Rubio, P., Rubio, L. et al.,“Determination of the Stress Intensity Factor of an elliptical breathing crack in a rotating shaft,”*Int J Fatigue*.,Vol. 77, pp. 216–31 (2015).

Rubio, P., Bernal, J., Muñoz-Abella, B. et al.,“A closed expression for the Stress Intensity Factor of concave fatigue cracks in rotating shafts,”*Engineering Fracture Mechanics*.,Vol. 214, pp. 233-247 (2019).

Saber El Arem.,“On the mechanics of beams and shafts with cracks: A standard and generic approach,”*European Journal of Mechanics / A Solids*.,Vol. 85, 104088 (2021).

Sekhar, A. and Prabhu, B.S.,“Vibration and stress fluctuations in cracked shafts,” *J. of sound and vibration*.,Vol. 169, pp. 655-667 (1994).

Sladek, J., Sladek, V. et al.,“Contour integrals for mixed-mode crack analysis: effect of nonsingular terms,” *Theor and app. Frac. mech*.,Vol. 27, pp. 115-127 (1997).

Sony, S. and Paulino, G.,“Dynamic stress intensity factors for homogeneous and smoothly heterogeneous materials using the interaction integral method,”*Int. J. of Sol. and Str*.,Vol. 43, pp. 4830- 4866 (2006).

Theocaris, P. and Ioakimidis, N., “Stress intensity factors and complex path-independent integrals,” *J. of App. Mech*., Vol. 47, pp. 342-346 (1980).

NOMENCLATURE

a	Crack length (mm)
d	Diameter of shaft (mm)

E	Elasticity modulus (GPa)
$\overline{F}_t$	Fictive force vector (N)
f_i	Effort term (N)
G	Shear modulus (GPa)
I_p	Polar quadratic moment (mm4)
$[K]$	Stiffness matrix (N.m^{-1})
$[K^*]$	Fictive stiffness matrix (N.m^{-1})
K_{III}	Stress intensity factor (MPa.m$^{1/2}$)
k_{ij}	Stiffness term (N.m^{-1})
k^*_{ij}	Fictive stiffness term (N.m^{-1})
l	Shaft length (mm)
$[M]$	Mass matrix (Kg)
m	Moment per unit length (Nm.m^{-1})
m_{ij}	Mass term (Kg)
M_0	External torque (Nm)
mt	Torsional moment (Nm)
$\underline{q}(t)$	Generalized displacement vector (mm)
$\dot{\underline{q}}_t$	Generalized speed vector (rd.s^{-1})
$\ddot{\underline{q}}_t$	Generalized acceleration vector (rd.s^{-2})
R	Shaft radius (mm)
S	Shaft section (mm^2)
T	Kinetic energy (J)
t	Time (s)
U	Potential strain energy (J)
W	Work of the external moment (J)
x_c	Crack position (mm)
x_m	Moment position (mm)
Y	Correction factor
β	NewMark’s parameter
γ	NewMark’s parameter
δ	Dirakfonction
Δt	Time increment (s)
ω	Frequency (s^{-1})
μ	Relative lengths of cracks
ρ	Density (Kg.m^{-3})
τ	Nominal shear stress (MPa)
σ_{ij}	Stress field (MPa)
ϕ	Deformation angle (rd)